K-9-04
Extended Abstracts of the 2020 International Conference on Solid State Devices and Materials, VIRTUAL conference, 2020, pp751-752

# Different Wavelength Photon Emissions from Group-IV-Semiconductor Quantum-Dots Fabricated by Hot-Ion Implantation Technique

**T. Mizuno, R. Kanazawa, K. Yamamoto, K. Murakawa, K. Yoshimizu, M. Tanaka, T. Aoki, and T. Sameshima***
Kanagawa Univ., Hiratsuka, Japan (mizuno@kanagawa-u.ac.jp), * Tokyo Univ. of Agric. and Tech., Koganei, Japan

## Abstract

**We experimentally studied three types of group-IV-semiconductor quantum-dots (IV-QDs) of Si-, SiC-, and C-QDs in Si-oxide (OX) layer fabricated by very simple process of hot-ion implantation technique of $Si^+$, double $Si^+/C^+$, and $C^+$ into OX, respectively, to realize a different wavelength PL emission from near-IR to near-UV ranges. TEM analyses newly confirmed both Si- and C-QDs with a diameter of ~2nm in OX. We can successfully demonstrate very strong PL emission from three IV-QDs, and the peak photon energies $E_{PH}$ (peak wavelength) of Si-, and SiC-, and C-QDs were approximately 1.56eV (880nm), 2.5eV (500nm), and 3.3eV (380nm), respectively. IV-QDs showed that PL properties strongly depend on the hot-ion doses of Si and C atoms and the post $N_2$ annealing processes. Consequently, it is easily possible for IV-QDs to design peak PL emission wavelength by controlling the ion doses of $Si^+$ and $C^+$ implanted into OX layer.**

## I. Introduction

Using the self-clustering effects of hot ion-implanted C atoms in Si layer [1], 3C-SiC and hexagonal-SiC (H-SiC) nano-dots (diameter $R\approx$2nm) can be easily formed in various Si crystal structures from amorphous to crystal Si by hot-$C^+$-ion implantation technique [2], [3]. We demonstrated very strong PL emission $I_{PL}$ in near-UV/visible regions (>400nm) from indirect-bandgap SiC-dots, which is attributable to free exciton recombination of excited electrons in SiC-dots [4]. However, since the SiC dots with larger bandgap $E_G$ (>2.4eV) are embedded in Si layer with smaller $E_G$ ($\approx$1.1eV), the SiC-dots in Si layer is not a quantum-dot (QD), resulting in too small PL quantum efficiency for visible Si-based photonic devices. Thus, we experimentally realized SiC-QDs embedded in $SiO_2$ (OX) with large $E_G\approx$9eV, using double hot-$Si^+/C^+$-ion implantation into an OX [5]. We successfully confirmed that the PL quantum efficiency of SiC-QDs is 2.5 times higher than that of SiC-dots in Si, because of enlarged life time of electrons which are quantum mechanically confined in SiC-QDs [5]. Thus, to realize different wavelength photonic devices from IR to UV range, QD structures with various $E_G$, such as Si- and C-QDs except SiC-QDs are strongly required, too. C- and Si-QDs have been widely studied [6], [7], but have been not realized by very simple and ULSI compatible processes of hot-ion implantation technique, yet.

In this work, we experimentally studied group-IV-semiconductor QDs (IV-QDs) of Si-, SiC-, and C-QDs, using very simple processes of hot-ion implantation into OX layer and the post $N_2$ annealing. We successfully demonstrated very strong PL emissions with different peak photon energies $E_{PH}$ from Si-QDs (near-IR (NIR)) by $Si^+$ hot-implantation, SiC-QDs (visible range) by double $Si^+/C^+$ hot-implantation [5], and C-QDs (near-UV) by $C^+$ hot-implantation.

## II. Experiment Procedure

Using the simple fabrication processes of hot-ion implantation into an OX layer and post $N_2$ annealing [5], we realized three types of IV-QDs (Si-, SiC-, and C-QDs) in OX layer. For example, Si-QDs ($Si^+$-OX) were fabricated by hot-$Si^+$ implantation into the OX layer on (100) bulk-Si substrate at substrate temperature $T$ (600°C) **(Fig.1(b))** after forming 140-nm thick OX by dry $O_2$ of Si **(Fig.1(a))**. Post $N_2$ annealing was carried out at annealing temperature $T_N$=1000°C for various annealing time $t_N$ **(Fig.1(c))**. Moreover, SiC- ($Si^+/C^+$-OX) and C-QDs ($C^+$-OX) were also fabricated by double hot $Si^+/C^+$ and single hot $C^+$ implantation into OX [5] at various $T$, respectively, instead of single hot $Si^+$ ion implantation in Si-QDs **(Fig.1(b))**. In this study, hot-ion dose conditions of $Si^+$ ($D_S$) and $C^+$-ion doses ($D_C$) were varied from $4\times10^{16}$ to $1\times10^{17}$ $cm^{-2}$ for increasing the PL intensity of IV-QDs.

PL and Raman properties of IV-QDs were measured at room temperatrure, where the excitation laser energy and diameter were 3.8eV and 1µm, respectively. The wide photon wavelength $\lambda_{PL}$ PL spectrum from the near-UV (NUV) to NIR regions was calibrated using a standard illuminant.

## III. Results and Discussions

### *A. Material Structures of IV-QDs*

The depth profiles of implanted atom concentration in IV-QDs was evaluated by XPS, and the peak Si at $D_S$=$6\times10^{16}$$cm^{-2}$ and C concentrations at $D_C$=$4\times10^{16}$$cm^{-2}$ were approximately $6\times10^{21}$ and $4\times10^{21}$$cm^{-3}$, respectively (**Fig.2**). We successfully confirmed many Si- (**Fig.3(a)**) and C-QDs (**Fig.3(b)**) in OX by HAADF-STEM, too, and SiC-QDs were already verified in our previous work [5]. Moreover, clear lattice spots of SiC-, Si-, and C-QDs can be observed by CSTEM (**Fig.4**). The average diameters $R$ of IV-QDs were approximately 2-4nm (**Fig.5**). Moreover, IV-QD densities $N$ were around $2\times10^{12}$$cm^{-2}$ (**Fig.5**).

### *B. Raman Properties*

UV-Raman of Si-QDs shows that an a-Si Raman peak decreases with increasing $t_N$ (**Fig.6(a)**), which indicates that the crystal quality of Si-QD can be improved by $N_2$ annealing. Moreover, the G- and D-bands of C-C vibrations in C-QDs also increases with increasing $t_N$ (**Fig.6(b)**), and thus graphite-based C-QD quality also increases after $N_2$ annealing. The Raman spectrum of SiC-QDs strongly depends on the dopant ratio of $D_S/D_C$, and both the TO of Si-C vibration and D-band intensity increase with decreasing $D_S/D_C$ even at the same $D_C$ **(Fig.7)**.

### *C. PL Properties*

We experimentally demonstrated the different $E_{PH}$ ($\lambda_{PL}$) emissions from C-QDs (NUV), SiC-QDs (visible region), and Si-QDs (NIR) **(Fig.8)**. The $I_{PL}$ of SiC-QDs was largest, and approximately 2.5 and 7.0 times as large as that of Si- and C-QDs, respectively. Moreover, Si-QDs shows very sharp PL spectrum with FWHM of 0.23eV, compared with broad PL spectra of SiC- (0.85eV) and C-QDs (0.89eV). Consequently, it is easily possible for IV-QDs to control PL emission wavelength from NIR to NUV by changing the atom implanted into OX.

The peak-$I_{PL}$; $I_{MAX}$ of IV-QDs rapidly increases after short $N_2$ annealing **(Fig.9)**, which is possibly attributable to the increase of the improved crystal quality of IV-QDs **(Figs.6(a), 6(b))**. In addition, even at the high-$T_N$ annealing, the $I_{MAX}$ of IV-QDs does not degrade after long $t_N$, which was confirmed even at $T_N$=1200°C. However, SiC-dots in Si layer (dotted line in (**Fig.9**) shows the drastic decrease of $I_{MAX}$ with increasing $t_N$ at $T_N\geq$900°C, which suggests that SiC-dots in Si is thermally instable [3]. Thus, IV-QD structures have thermal stability in $T_N$ of lower than at least 1200°C, which is the advantageous characteristic of QDs in OX.

The $I_{MAX}$ and $E_{PH}$ ($\lambda_{PL}$) of Si- and C-QDs also depend on $D_S$ and $D_C$, respectively **(Fig.10)**. With increasing the ion dose, the $I_{MAX}$ of Si-QDs decreases, but the $I_{MAX}$ of C-QDs increases. In addition, the $E_{PH}$ of Si-QD is almost independent of $D_S$, but the $E_{PH}$ of C-QDs increases with increasing the $D_C$.

On the other hand, the PL spectrum of SiC-QDs strongly depend on the $D_S/D_C$ ratio even at fixed $D_C$ **(Fig.11)**. Namely, the $I_{MAX}$ of SiC-QDs rapidly decreases at $D_S/D_C$=2, because of reduced Si-C bonding **(Fig.7)**. In addition, the $E_{PH}$ of SiC-QD decreases with increasing $D_S/D_C$.

Consequently, the peak-$\lambda_{PL}$ of IV-QDs from NUV to NIR regions can be easily designed by $D_S$ and $D_C$ conditions **(Fig.12)**. Namely, shorter or longer $\lambda_{PL}$ emissions of IV-QDs can be achieved by increasing $D_C$ or $D_S$, respectively **(Fig.12)**.

## IV. Conclusion

In this work, we experimentally studied group-IV semiconductor -QDs (Si-, SiC-, and C-QDs) in OX layer, fabricated by hot-ion implantation and the post $N_2$ annealing. We demonstrated very strong PL emissions from IV-QDs with different $\lambda_{PL}$ of NIR from Si-QDs, visible range from SiC-QDs, and NUV from C-QDs. Thus, it is easily possible for IV-QDs to design peak-$\lambda_{PL}$ by controlling ion doses of Si, Si/C, and C implanted into OX layer.

**Acknowledgement:** This work was partially supported by KAKENHI (17K06359).

**References:** [1] T.Mizuno, JJAP **57**, 04FB03, 2018. [2] T.Mizuno, JJAP **58**, SBBJ01, 2019. [3] T.Mizuno, JJAP **58**, 081004, 2019. [4] J.Fan, *Silicon Carbide Nanostructures* (Springer), 2014. [5] T.Mizuno, JJAP **59**, SSGH02, 2020. [6] N.Yang, *Carbon Nanoparticles and Nanostructures*, (Springer), 2016. [7] L.Pavesi, *Silicon Nanocrystal*, (Wiley-VCH), 2010.

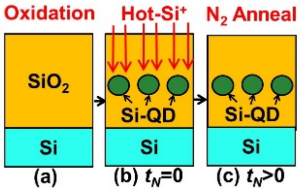


**Fig.1** Si-QD fabrication steps in $Si^+$-OX by hot-$Si^+$-ion-implantation into $SiO_2$ layer. After (a) dry-oxidation process of bulk-Si substrate, (b) hot-$Si^+$-ions with $D_S$ were implanted into $SiO_2$ layer at $T$. (c) Post $N_2$ annealing was carried out at $T_N$ for $t_N$.

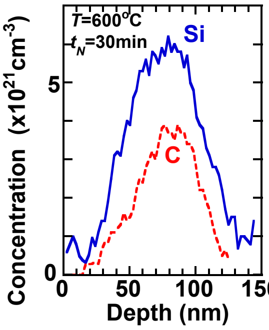


**Fig.2** Concentration depth profiles of implanted Si (solid line) at $D_S$=6×10$^{16}$cm$^{-2}$ or C (dashed line) atoms at $D_C$=4×10$^{16}$cm$^{-2}$ in $SiO_2$ layer, which was evaluated by Si2p and C1s spectra of XPS, respectively, where $T$=600°C and $t_N$=30min.

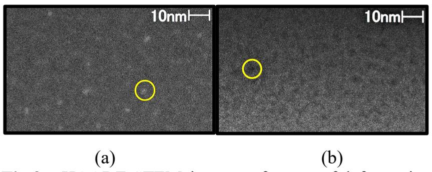


**Fig.3** HAADF-STEM images of successful formation of many (a)Si-QDs (encircled bright spot) at $D_S$=6×10$^{16}$ cm$^{-2}$, $T$=600°C and $t_N$=60min, and (b) C-QDs (encircled dark spot) at $D_C$=1×10$^{17}$ cm$^{-2}$, $T$=400°C and $t_N$=30min

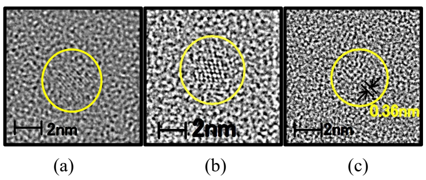


**Fig.4** CSTEM lattice images of (a) hexagonal-SiC-QD at $D_S$=6×10$^{16}$ cm$^{-2}$, $D_C$=4×10$^{16}$cm$^{-2}$, $T$=400°C, and $t_N$=30min, (b) Si-QD, and (c) C-QD. Process conditions of (b) and (c) are the same of Fig.3. The lattice distance of C-atoms in (c) was approximately 0.36nm, which is nearly equal to the layer distance of graphite (0.335nm).

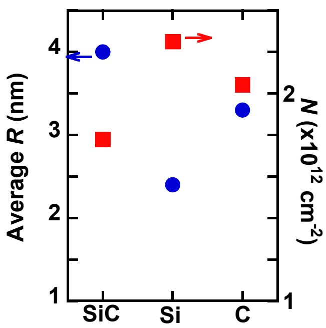


**Fig.5** Average $R$ (circles) and $N$ (squares) of SiC-QDs ($D_S$=6×10$^{16}$cm$^{-2}$, $D_C$=4×10$^{16}$cm$^{-2}$, $T$=600°C, and $t_N$=30min), Si-QDs and C-QDs. Process conditions of Si- and C-QDs are the same as those of Fig.3.

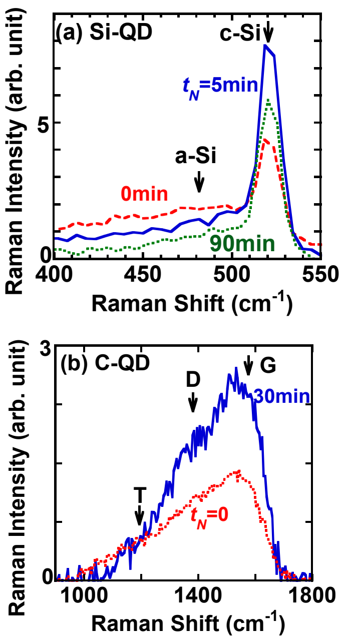


**Fig.6** $t_N$ dependence of UV-Raman spectra of (a) Si-QD at $D_S$=6×10$^{16}$cm$^{-2}$, and (b) C-QD at $D_C$=1×10$^{17}$ cm$^{-2}$, where $T$=600°C. The arrows in (a) show the peak Raman shifts of c-Si (520cm$^{-1}$) and a-Si (480cm$^{-1}$). The arrows in (b) show the T, D, and G bands of C-C vibration.

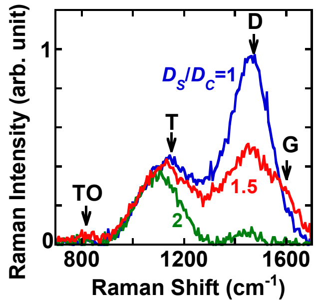


**Fig.7** $D_S$/$D_C$–ratio dependence of Raman spectra of SiC-QD at fixed $D_C$=4×10$^{16}$cm$^{-2}$, where $T$=200°C, and $t_N$=0. The arrows show the G, D and T bands of C-C vibrations, and the TO mode of Si-C vibration.

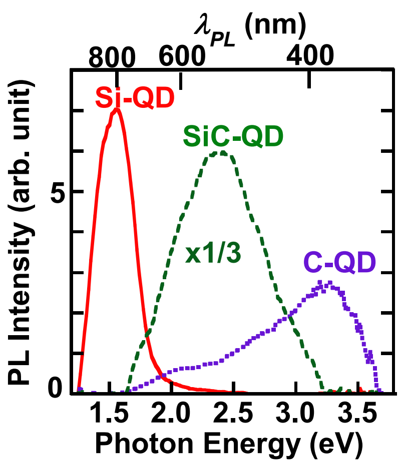


**Fig.8** PL spectrum comparison between Si-QD (solid line: $D_S$=6×10$^{16}$cm$^{-2}$, $T$=600°C, $t_N$=1.5h), SiC-QD (dashed line: $D_S$=6×10$^{16}$cm$^{-2}$, $D_C$=4×10$^{16}$cm$^{-2}$, $T$=200°C, $t_N$=30min), and C-QD (dotted line: $D_C$=1×10$^{17}$cm$^{-2}$, $T$=600°C, $t_N$=30min). The lower and upper axes show the PL photon energy and wavelength, respectively. The PL intensity of SiC-DQ shows 1/3 times as large as measured PL data.

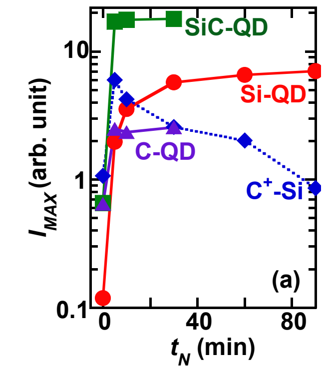


**Fig.9** $t_N$ dependence of $I_{MAX}$ as the same data of Fig.8 (Si-QD (circles), SiC-QD (squares), and C-QD (triangles)). Rhombi show the data of SiC dots in Si layer ($C^+$-Si).

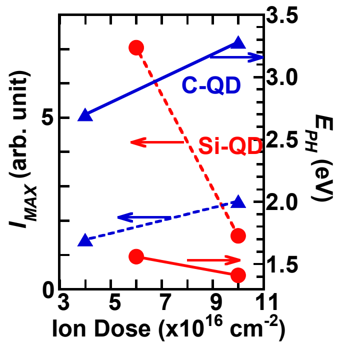


**Fig.10** Ion dose dependence of $I_{MAX}$ (dashed lines) and $E_{PH}$ (solid lines) of Si-QD (circles) and C-QD (triangles) after $N_2$ annealing, where $T$=600°C.

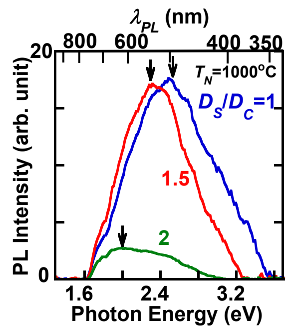


**Fig.11** $D_S$/$D_C$–ratio dependence of PL spectrum of SiC-QD at $t_N$=5min, where $D_C$=4×10$^{16}$cm$^{-2}$ and $T$=200°C. Arrows show the $E_{PH}$ positions.

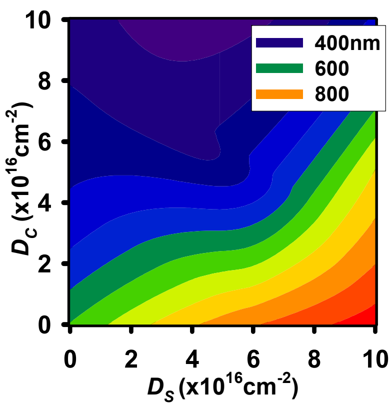


**Fig.12** $D_S$/$D_C$ conditions for designing peak-$\lambda_{PL}$ of IV-QDs. This contour map of peak-$\lambda_{PL}$ was obtained by the data of Figs. 8, 10, and 11.